Heat Source and Activation Energy effects on 3D Couple Stress Casson Fluid Motion via Stretching Sheet

K. Bharathi [1,2,*], Maddileti Pasupula[3], Motamari Madhu[4,5]

1 Assistant Professor, Department of Mathematics, University PG Centre Palamuru University, Kollapur-509102, Telangana, India*

2 Research Scholar, Department of Mathematics, Bhartiya Engineering Science and Technology Innovation University (BESTIU), Mandrol Lakeside Campus, Sri Satya Sai District-515321, A.P, India*

[3]Departemnt of Mathematics, University College of Science, Mahatma Gandhi University, Nalgonda, Telangana, India

[4]Department of Mathematics, University College, Palamuru University, Mahabubnagar-509001, Telangana, India

Abstract: -The proposed study is significant importance due to more applications in bullets and aircrafts, drilling processes, biological treatments, food processing, manufacturing process of submarine, bio-engineering activities, and many engineering and industrial works like heating and cooling processes and chemical works. The aim of present work is to scrutinize the motion, HMTR for BL of CSC nanofluid (NFs) with NLTR, heat source and AE via SS. The compatible similarity variables are used to convert governing equations of considered liquid model occurred in the PDEs into ODEs form and then calculated through "Range-Kutta-Fehlberg" 4th order algorithm with shooting technique. The physical parameters are plotted graphical representation in terms of $f'(\eta)$ ("Axial direction"), $g'(\eta)$ ("Transverse direction"), $\phi(\eta)$ ("Concentration") as well as HMTR, and coefficient of skin friction. We found that, the concentration of couple stress NFs have more in presence of AE and skin friction coefficient is more in CSC NFs for higher porous parameter. The numerical solutions are comparing into some of previous articles, then we get good revolution of numerical values.

Keywords: *Activation Energy, Heat Source, Couple Stress.*

Introduction

The phenomenon of liquid motion across a stretching sheet indeed holds significant relevance in various fields of science and engineering. The SS configuration serves as a fundamental model for studying fluid dynamics and has wide-ranging applications, In the production of paper and glass, the process often involves the controlled movement of liquid materials across a surface. Understanding the dynamics of liquid flow on a SS is crucial for optimizing these manufacturing processes, ensuring uniformity, and controlling material properties. Similarly, in the extrusion of melting polymers through a slit die, the behavior of the polymer melts as it passes through the die is influenced by the stretching action of the die. This stretching process affects the final properties of the extruded product, such as thickness, surface finish, and mechanical properties. By studying the motion of the polymer melt on the stretching sheet, engineers can improve the design of extrusion processes for various applications like wire drawing and plastic sheet production. One important aspect to note is that the velocity of the liquid on the stretching sheet is not always linear. This non-linearity introduces complexity into the fluid dynamics of the system. Researchers are interested in understanding and characterizing these non-linear behaviours to develop accurate predictive models and control strategies for industrial processes. Saeed et al. [1] developed the HNFs enhanced 11.95% HTR. Alghamdi et al. [2] proposed the MHD and heat source or sink on flow pattern. Raja Sekhar et al. [3] developed a model called Walter's liquid-B model NFs via SS.

Mabood et al. [4] demonstrated entropy minimization can be accomplished by decreasing MF, Prandtl, Eckert and Schmidt numbers as well as NPs volume fraction. The HMTR of MHD Williamson NFs motion past a PSS. With TR and CR. Li et al. [5] found that, the high entropy rate is found against magnetic PN. Li et al. [6] presented the slip velocity declined the motion speed while temperature of NFs was observed to be more. Chu et al. [7] developed HNFs motion via SS. Recently, some authors [8-11] developed numerical study on HNFs motion with various physical effects. Algehyne et al.[12]created numerical analysis of SHNFs motion via heated shrinking or SS with porous disk. Bilal et al. [13] examined ternary HNFs by help of variable diffusion and non-Fourier's.

Thermal conductivity of nanofluids refers to the ability of these suspensions containing nanoparticles (usually metallic or non-metallic) dispersed in a base fluid to conduct heat. The presence of NPs in the fluid alters its thermal properties compared to the base fluid alone. The TC enhancement in NFs can be attributed to several factors, like **Particle Material** (silver, or gold), **Particle Size, Volume Fraction, Thermal Interface Resistance, Brownian Motion and Agglomeration, Interfacial Layer Formation**.The thermal conductivity of NFs was first investigated by Choi and Eastman [14]. Recently, some of the authors [15-17] investigated the HNFs motion with various HT effects by using HAM algorithm. Nasir et al. [18] presented the HNFs motion with nonlinear TR. Li et al. [19] explored the Darcy-Forchheimer and AE parameters are boosted, the liquid speed and concentration has declined. Harshavardhan et al. [20] presented the SnO_2 NPs are prepared via environmental BM ("Benign Method") by help of nelumbo nucifera leaves.

MHD is a branch of physics that deals with the study of the comportment of EC liquids such as plasmas, liquid metals, and saltwater when subjected to magnetic fields. This interdisciplinary field combines principles from fluid dynamics and electromagnetism to understand phenomena such as the generation of electric currents in conductive fluids, the interaction between magnetic fields and fluid motion, and the behavior of plasma in fusion reactors and astrophysical environments. Applications of MHD span a wide range of fields including EPG, space propulsion, astrophysics, and materials processing. One notable example is magnetohydrodynamic power generation, where electric power is generated directly from the movement of conducting fluids in the presence of magnetic fields, eliminating the need for mechanical moving parts like turbines. MHD also plays a crucial role in understanding natural phenomena such as solar flares, the behavior of planetary magnetospheres, and the dynamics of accretion disks around black holes. Sivakumar et al. [21] presented numerical computation for Casson NFs via SS. Sivakumar and Rushi Kumar [22] explored the unsteady radiative motion with variable conductivity. Harish Babu et al. [23] examined the MHD motion of Jeffrey liquid via SS. Khashi'ie et al. [24] explored the MHD BL motion of HNFs via SS. Bourcy et al. [25] consider the effect on transient growth of spanwise magnetic field in BL motion of liquid metal via EI flat plate. Murad et al. [26] consider the MHD BL motion via NLSS. Nasir et al. [27] incorporated the MF, NUHG, DF porous space, Dissipation, OH and CR and AE into motion distribution. Jaafar et al. [28] explore the NLSS HNFs in terms of steady motion of HT with MHD, TR. Gul et al. [29] present the innovative idea of MHD unsteady, incompressible NFs motion via SRD (Stretching Rotating Disk). Ahmad et al. [30] examined the behaviour of AE, bio convectional, and gyrotactic microorganism phenomena in Oldroyd B liquid motion via RD (Rotating Disc).

non-Newtonian NFs are suspensions of NPs in a non-Newtonian (NN) base fluid, where the behavior of the mixture deviates from the traditional Newtonian liquid behavior. In Newtonian liquid, the viscosity remains constant regardless of the applied stress, while in NN liquids, the viscosity changes with the applied stress or shear rate SR. The addition of nanoparticles to the base fluid alters its rheological properties, leading to enhancements in TC, viscosity, and other relevant characteristics. Applications of NN NFs include thermal management in electronics, enhanced oil recovery, drug delivery systems, and advanced manufacturing processes. However, challenges such as nanoparticle dispersion, stability, and scalability need to be addressed for widespread commercial adoption. Bhagya Lakshmi et al. [31] presented the MHD Casson liquid motion via CS. Satya Narayana et al. [32] exhibited the NLTR on three-dimensional motion of CSC NFs via SS. The MHD Radiative Casson nanofluids (CNFs) motion via SS with CR was presented by Sandhya et al. [33]. Priam and Nasrin et al. [34] found the mean temperature about 6.39 percentage is reduced due to shear transformation of

Casson liquid from thickening to thinning. The effect of thermal energy (TE) in terms of heat source (HS), thermal radiation (TR) and CR on MHD-CFM via nonlinear slanted extending surface was examined by Shoaib et al. [35]. Recently, the brilliant scientists [36-40] are presented the MHD motion of CNFs via SS. Raghunath and Obulesu et al. [41] performed the hydrodynamic motion via inclined plate with MF and CR. Bilal et al. [42] developed the energy transmission via ML was applied in the field of electronics, textiles, spacecraft, PG and NPP. Algehyne et al. [43] presented the hydrodynamic motion of WBNFs included motile microbes and nanomaterials via MS (Moving Surface).

The activation energy (AE) of a process in NFs can be influenced by various factors, including NPs size, shape, surface chemistry, and the properties of the base fluid. Understanding the AE is crucial for optimizing the synthesis and stability of NFs and for predicting their behavior under different conditions. Experimental techniques such as differential scanning calorimetry (DSC) or thermal analysis can be used to measure AE associated with processes occurring in NFs. Computational methods, such as molecular dynamics simulations, can also provide insights into the AE involved in NPs interactions and their effect on nanofluid properties. Overall, the study of AE in NFs is important for both fundamental understanding and practical applications, as it helps in designing NF systems with tailored properties for specific purposes. Sandhya et al. [44] examined the AE on MHD and radiative liquid motion with second order slip via ESS. Malleswari et al. [45] presented the suspension of NPs in a CR micropolar liquid motion via SS with CH and AE. Atwell et al. [46] performed the CR for which barriers are modeled included organic molecules, aromatic rings and organometallic catalysts. Azam et al. [47] observed the role of AE, nanoparticles and gyrotactic microorganisms with bioconvection uses in engineering oil reservoir, HT, CE. Some of scientists [48-50] developed the AE on bioconvection NFs with various effects via various geometrical models. Also, recently [51-53] explored the CNFs motion with AE via rotating and linear SS. Li et al. [54] motivated the upcoming scientists for selecting generalized micropolar liquid model are justifies as captures micropolar liquid, second grade liquid and viscous liquid results. Dhlamini et al. [55] investigate the BL motion of steady viscous NF wit AE and high order CR. Samuel et al. [56] performed the impact of AAE and binary reaction on HMT of MHD Jefrey liquid motion with non-uniform heat generation (HG), TR, and VS. Recently, some of authors [57-59] presented the HNFs motion under AE via SS. Thammanna et al. [60] exhibited the CSS liquid via unsteady SS.

1. Mathematical Analysis

Consider the 3D steady, incompressible, HG, TR, CR, AE, and MHD couple stress NFs motion is sustained to pass the LSS. The EC is considered in direction of liquid motion with MF M_0 can be applied in $z_1 > 0$. The liquid motion in porous stretching sheet at $z_1 = 0\ (z_1 > 0)$. The stretching velocities $u_1 = U_w(x^*) = a_1 x^*,\ u_2 = V_w(x^*) = b_1 y^*$ along in x^* and y^* directions. These are considering a Cartesian coordinate system for the purpose of representing liquid motion as visualised in Fig. 1. The rheological equation of Casson liquid for steady motion as taken by (see ref 61-63]):

$$\tau_{ij} = \begin{cases} \left(2\mu_0^* + \dfrac{2p_y^*}{\sqrt{2\pi^*}}\right)e_{ij}, & if\ \pi^* \geq \pi_1^* \\ \left(2\mu_0^* + \dfrac{2p_y^*}{\sqrt{2\pi_1^*}}\right)e_{ij}, & if\ \pi^* < \pi_1^* \end{cases}$$

(1)

Where, $p_y^* = e_{ij}e_{ij}$ and $\beta = \mu_B^*\sqrt{2\pi_1^*}/\mathrm{p}_y^*$. The fundamental equations of continuity, heat and concentration Eqs can be formulated by using eq. (1) as shown below ref. **[**63-65**]** and ref. [66-67]:

$$\frac{\partial u_1}{\partial x^*}+\frac{\partial v_1}{\partial y^*}+\frac{\partial w_1}{\partial z^*}=0 \tag{2}$$

$$u_1\frac{\partial u_1}{\partial x^*}+v_1\frac{\partial u_1}{\partial y^*}+w_1\frac{\partial u_1}{\partial z^*}=\upsilon^*\left(1+\frac{1}{\beta}\right)\frac{\partial^2 u_1}{\partial\left(z^*\right)^2}-\left(\upsilon^*\right)'\frac{\partial^4 u_1}{\partial\left(z^*\right)^4}-\frac{\sigma^* M_0^2}{\rho}u_1-\left(1+\frac{1}{\beta}\right)\frac{\upsilon^*}{k_p}u_1 \tag{3}$$

$$u_1\frac{\partial v_1}{\partial x^*}+v\frac{\partial v_1}{\partial y^*}+w\frac{\partial v_1}{\partial z^*}=\upsilon^*\left(1+\frac{1}{\beta}\right)\frac{\partial^2 v_1}{\partial\left(z^*\right)^2}-\left(\upsilon^*\right)'\frac{\partial^4 v}{\partial\left(z^*\right)^4}-\frac{\sigma^* M_0^2}{\rho}v_1-\left(1+\frac{1}{\beta}\right)\frac{\upsilon^*}{k_p}v_1 \tag{4}$$

$$u_1\frac{\partial T^*}{\partial x^*}+v_1\frac{\partial T^*}{\partial y^*}+w_1\frac{\partial T^*}{\partial z^*}=\alpha_m^*\frac{\partial^2 T^*}{\partial\left(z^*\right)^2}-\frac{1}{(\rho C^*)_f}\frac{\partial q_r}{\partial z^*}-\frac{Q_0}{(\rho C^*)_f}(\mathrm{T}^*-\mathrm{T}_\infty^*) \tag{5}$$

$$u_1\frac{\partial C^*}{\partial x^*}+v_1\frac{\partial C^*}{\partial y^*}+w_1\frac{\partial C^*}{\partial z^*}=D^*\frac{\partial^2 C^*}{\partial\left(z^*\right)^2}-K_1(\mathrm{C}^*-\mathrm{C}_\infty^*)-K_r^2\left(C_1-C_\infty\right)\left(\frac{T_1}{T_\infty}\right)^m\exp\left(\frac{-E_1 a_1}{k_1 T_1}\right)$$

(6)

The present relevant model boundary conditions as

$$\begin{aligned}&z^*=0\quad at\quad u_1=a_1x^*\quad \mathrm{v}=b_1y^*\quad \mathrm{w}_1=0,\ -k\frac{\partial T^*}{\partial z^*}=h_1(\mathrm{T}_f^*-\mathrm{T}^*)\quad -D^*\left(\frac{\partial C^*}{\partial z}\right)=h_2\left(C_f^*-C^*\right)\\&z^*\to\infty\quad as\quad u_1\to 0\quad \mathrm{v}_1\to 0,\ u_1'\to 0,\ \mathrm{v}_1'\to 0,\ T^*\to T_\infty^*,\ C^*\to C_\infty^*\end{aligned} \tag{7}$$

The similarity transformations as below

$$\left.\begin{aligned}&\eta_1=\sqrt{\frac{a_1}{\upsilon_f^*}}z^*,\quad u_1=a_1x^*f'(\eta_1),\quad v_1=a_1y^*g'(\eta_1),\quad \mathrm{w}_1=-\sqrt{a_1\upsilon^*}\left(f(\eta_1)+g(\eta_1)\right)\\&\theta(\eta_1)=\frac{T^*-T_\infty^*}{T_w^*-T_\infty^*},\quad \phi(\eta_1)=\frac{C^*-C_\infty^*}{C_w^*-C_\infty^*}\end{aligned}\right\}$$

(8)

Using above **Eq. (8)**, we are converting **Eq. (3)-(6)** into below format

$$Kf^v+f'''(1+\beta/\beta)+f''(f+\mathrm{g})-(f')^2-(\mathrm{M}+\Gamma(1+\beta/\beta))f'=0$$

(9)

$$Kg^v+g'''(1+\beta/\beta)+g''(f+\mathrm{g})-(g')^2-(\mathrm{M}+\Gamma(1+\beta/\beta))\mathrm{g}'=0$$

(10)

$$\theta''(1+\mathrm{R}_d(\theta(\theta-1)+1)^3)+\Pr(f+\mathrm{g})\theta'-HP\mathrm{r}\,\theta=0 \tag{11}$$

$$\phi''=\sigma_2(1+\delta\theta)^n\exp\left(-E_1/1+\delta_1\theta\right)\phi-\Pr Le\left((f+\mathrm{g})\phi'-\gamma\phi\right) \tag{12}$$

Corresponding B.Cs. as below

$$\left.\begin{aligned}&f=0,\quad g=0,\quad f'=1,\quad g'=\lambda,\quad \theta'=-\Gamma_1(1-\theta),\quad \phi'=-\Gamma_2(1-\phi)\quad at\quad \eta_1=0\\&f'\to 0,\quad g'\to 0,\quad f''\to 0,\quad g''\to 0,\quad \theta\to 0,\quad \phi\to 0,\quad as\quad \eta_1\to\infty\end{aligned}\right\}$$

(13)

Moreover, the skin-friction coefficient and Nusselt number are below

$$\left.\begin{aligned}&C_{fx}=(1+\frac{1}{\beta})f''(0)\mathrm{Re}_x^{-1/2}-\mathrm{K}\,f^v(0)\mathrm{Re}_x^{-1/2},\quad C_{fy}=(1+\frac{1}{\beta})\mathrm{g}''(0)\mathrm{Re}_x^{-1/2}-\mathrm{K}\mathrm{g}^v(0)\mathrm{Re}_x^{-1/2}\\&Nu_x=-\left(1+R_d(\theta(\theta_w-1)+1)^3\right)\theta'(0)\mathrm{Re}_x^{1/2}\end{aligned}\right\}$$

(14)

Tuijin Jishu/Journal of Propulsion Technology
ISSN: 1001-4055
Vol. 45 No. 2 (2024)

2. Results and Discussion

Fig. 2 which explores the result of the applied magnetics force on $f'(\eta_1)$ and $g'(\eta_1)$. The M is placed perpendicular to the direction of liquid motion causes a falloff in the output of both velocity (like, $f'(\eta_1)$ and $g'(\eta_1)$) directions. The high velocity of CS NFs motion in porous surface with effect of AE. physically, the field of MF effects creates the resistive forces which make the internal friction that affects moves to high velocity in surface area and also, the BL converges very near to the SS in between $0 \le \eta_1 \le 2$ region.

The β on $f'(\eta_1)$ and $g'(\eta_1)$. was explained graphically as predict in Fig. 3. The parameter of CF rises with enlarge numerical values of β due to high dynamic viscosity of CNFs motion at surface area. Physically, the yield stress of CF diminished because low resistance of CSCNFs. Thus, the outcome of increasing the value of Casson parameter gives a declined at region $0.2 \le \eta_1 \le 1$ for axial velocity and $1 \le \eta_1 \le 1.2$ for transverse velocity.

Fig. 4 analysed the variations of K on $f'(\eta_1)$ and $g'(\eta_1)$. It is clear that, the velocity is enhanced more for large numerical values of K. Physically, the high viscosity of CSCNFs motion in surface area, due to this reason, we get conclusion of the velocity profiles diminishes at surface area $0.2 \le \eta_1 \le 1$ for higher values of K.

Figs. 5-6 gives the variations of $\Pr$, H on $\theta(\eta_1)$, respectively. The temperature dominates with increasing numerical values of $\Pr$. Physically, the $\Pr$ is a relationship between KV and TD. Hance, low thermal diffusivity produces low temperature of couple stress Casson nanofluid. Thus, the TBL converges to $0 \le \eta_1 \le 1.5$ more effective in pure fluid while comparing to Casson fluid BL with enlarge statistical values of $\Pr$. Enhancing value of H strengthens the BL of temperature. The temperature is high in motion of CF (because the increasing resistance in liquid raises the temperature on Casson fluid motion) higher than pure fluid for the increasing values of H as explored in Fig. 6.

The variations of Γ_1 on $\theta(\eta_1)$ was analysed by graphically as shown in Fig. 7. The Γ_1 analysed for temperature refers the relation between internal conductive resistance and convective resistance at $0 \le \eta_1 \le 1$. The enlarge statistical values of Γ_1 dominates the internal conductive resistance, that is temperature gets strengthened. So that, $\theta(\eta_1)$ raises for the case of CSCF while comparing to pure liquid motion. In Fig. 8 depicts the variation of E (AE) on $\phi(\eta_1)$. It is perceived that; the concentration is high in case of CSCF while compared to pure liquid for enlarge numerical values of E. The CSCF transforms released more viscous in liquid motion. so that, the concentration profile becomes slow.

Fig. 9 Shows variations of Le (Lewis number) on $\phi(\eta_1)$ with presence and absence of E (Activation Energy). The Lewis number is a relationship between thermal diffusivity and mass diffusivity, it is used to describe the motion liquid at surface. It assesses the relative concentration and thermal thickness of BL. Physically, A little quantity of energy is required for energies atoms or molecules for chemical reaction, but when the high AE gives enough energy for fewer atoms or molecules to react or collide, then reaction will become slow. Intensifying the value of the Lewis number with the presence of AE, the concentration profile will be enhanced while compared to absence of activation energy. Hence, the concentration will become high for enhancing Lewis number with presence of AE.

Fig. 10 explains the variations of $\Pr$ on the Nusselt number. Physically, the relation between the kinematic viscosity to the thermal diffusivity which often referred to as the Prandtl number. A larger value of the Prandtl number depicts that the kinematic viscosity dominates the flow of fluid, and with the presence of the Casson couple stress parameter gives the more viscous flow. Thus, here conductive heat transfer occurs for the pure fluid than the Casson fluid.

Fig. 11 shows the variations of H on the Nusselt number. Physically, Nusselt number is the relation between the thermal energy convection to the fluid to the thermal energy conducted within the fluid. The presence of Casson couple stress parameter yields more viscous to the fluid flow, with intensifying the value of the heat source parameter diminishing the heat rate in the convection energy profile than the Casson couple fluid parameter absence.

Fig. 12 Explains the variations of β on Skin friction ("via y^* axis"), respectively. There is a friction towards a solid surface and a relative motion of a fluid which refers the skin friction. Casson parameter gave viscous to the flow of fluid so that the higher value of this parameter gave lower skin friction for the absence of heat source parameter than its presences.

Figs. 13-14 shows the variations of a K on Skin friction ("via x^*, y^* axis"), respectively. While rising the value of K with the Casson parameter appearance both give more viscous to the flow fluid which diminishes the skin friction. Whereas the lack in the Casson parameter gives a vast difference in skin friction compared to its presence. Figs. 15-16 explains the variations of Γ on Skin friction ("via x^*, y^* axis"), respectively. Enlarging the values of porous (number of voids or pores) parameter which developing the more friction between the solid surface to the fluid in relative motion.

For checking the calculated statistical results in present work by bvp 4th order is matched up to the four decimal places and also obtained extended statistical values in current work is compared to related articles of [64], [65], [66], [67] for some specific cases (like $K = \lambda$=0 and λ=1.0) and getting good agreement results (see Table 1, 2), respectively.

3. Conclusion

We analysed Arrhenius Activation Energy on three-dimensional coupe stress non-Casson fluid via permeability stretching surface. Based on current work key analysis results are listed below:

- The concentration of couple stress Casson liquid is more in permeable SS with high numerical values of Le, E.
- The rate of heat transfer is more in Casson couple stress fluid while comparing with pure liquid for high heat generation.
- The coefficient of skin friction $\mathrm{Re}_x^{-1/2} C_{fy}$ is high impact along y*-direction in presence of heat generation while absence of heat generation.
- The liquid velocity is high in axial and transverse path for enlarge numerical values of couple stress parameter.

Refrences

[1] Saeed, A., Alsubie, A., Kumam, P., Nasir, S., Gul, T. and Kumam, W. Blood based hybrid nanofluid flow together with electromagnetic field and couple stresses, Scientific Reports, **11**, 12865 (2021).

[2] Alghamdi, W., Alsubie, A., Kumam, P., Saeed, P. and Gul, T. MHD hybrid nanofluid flow comprising the medication through a blood artery, Scientific Reports, **11**, 11621 (2021).

[3] Raja Sekhar, P., Sreedhar, S., Mohammed Ibrahim, S., Vijaya Kumar, P. and Omprakash, O. Numerical investigation of heat radiation on MHD viscoelastic nanofluid flow over a stretching sheet

with heat source and slip conditions, International Journal on Interactive Design and Manufacturing, (2023). https://doi.org/10.1007/s12008-023-01407-4.

[4] Mabood, F., Fatunmbi, E.O., Benos, L. and Sarris, I.E. Entropy Generation in the Magnetohydrodynamic Jeffrey Nanofluid Flow Over a Stretching Sheet with Wide Range of Engineering Application Parameters, International Journal of Applied and Computational Mathematicsvolume, **8**, 98 (2022).

[5] Patil, V.S., Humane, P.P. and Patil, A.B. MHD Williamson nanofluid flow past a permeable stretching sheet with thermal radiation and chemical reaction, International Journal of Modelling and Simulation, **43** (2023).

[6] Li, S., Khan, M.I., Alzahrani, F. and Eldin, S.M. Heat and mass transport analysis in radiative time dependent flow in the presence of Ohmic heating and chemical reaction, viscous dissipation: An entropy modeling, Case Studies in Thermal Engineering, **42**, 102722 (2023).

[7] Chu, Y.M., Khan, M.I., Abbas, T., Sidi, M.O., Alharbi, K.A.M., Alqsair, U.F., Khan, S.U., Khan, M.R. and Malik, M.Y. Radiative thermal analysis for four types of hybrid nanoparticles subject to non-uniform heat source: Keller box numerical approach, Case Studies in Thermal Engineering, **40**, 102474 (2022).

[8] Li, S., Puneeth, V., Saeed, A.M., Singhal, A., Al-Yarimi, F.A.M., Khan, M.I. and Eldin, S.M. Analysis of the Thomson and Troian velocity slip for the flow of ternary nanofluid past a stretching sheet, Scientific Reports, **13**, 2340 (2023).

[9] Raizah, Z., Alrabaiah, H., Bilal, M., Junsawang, P. and Galal, A.M. Numerical study of non-Darcy hybrid nanofluid flow with the effect of heat source and hall current over a slender extending sheet, Scientific Reports, **12,** 16280 (2022).

[10] Alrabaiah, H., Iftikhar, S., Saeed, A., Bilal, M., Eldin, S.M. and Galal, A.M. Numerical Calculation of Darcy Forchheimer Radiative Hybrid Nanofluid Flow across a Curved Slippery Surface, South African Journal of Chemical Engineering, **45** (2023) 172-181.

[11] Algehyne, E.A., Alrihieli, H.F., Bilal, M., Saeed, A. and Weera, W. Numerical Approach toward Ternary Hybrid Nanofluid Flow Using Variable Diffusion and Non-Fourier's Concept, ACS Omega, **7**(33) (2022) 29380-29390.

[12] Kumar Mishra, N., Anwar, S., Kumam, P., Seangwattana, T., Bilal, M. and Saeed, A. Numerical investigation of chemically reacting jet flow of hybrid nanofluid under the significances of bio-active mixers and chemical reaction, Heliyon, **9**(7) (2023) e17678. Doi: 10.1016/j.heliyon.2023. e17678.

[13] Bilal, M. and Saeed, A. Numerical computation for the dual solution of Sisko hybrid nanofluid flow through a heated shrinking/stretching porous disk, International Journal of Ambient Energy, **43**(1) (2022) 8802-8811.

[14] Choi, S.U.S. and Eastman, J.A. Enhancing Thermal Conductivity of Fluids with Nanoparticles, Argonne National Lab. (ANL), Argonne, IL, United States, (1995).

[15] Alnahdi, A.S., Nasir, S. and Gul, T. Blood-based ternary hybrid nanofluid flow-through perforated capillary for the applications of drug delivery, Waves in Random and Complex Media, (2022). https://doi.org/10.1080/17455030.2022.2134607.

[16] Bilal, M., Gul, T., Alsubie, A. and Ali, I. Axisymmetric hybrid nanofluid flow with heat and mass transfer amongst the two gyrating plates, ZAMM- Journal of Applied Mathematics and Mechanics, **101**, (2021).

[17] Rehman, A., Saeed, A. and Bilal, M. Analytical Study of Three-Dimensional MHD Hybrid Nanofluid Flow along with Thermal Characteristics and Radiative Solar Energy, Waves in Random and Complex Media, (2022). https://doi.org/10.1080/17455030.2022.2077472.

[18] Nasir, S., Berrouk, A.S., Aamir, A., Gul, T. and Ali, I. Features of flow and heat transport of MoS_2+GO hybrid nanofluid with nonlinear chemical reaction, radiation and energy source around a whirling sphere, Heliyon, **9**, e15089 (2023).

[19] Li, S., Raghunath, K., Alfaleh, A., Ali, F., Zaib, A., Khan, M.I., Eldin, S.M. and Puneeth, V. Effects of activation energy and chemical reaction on unsteady MHD dissipative Darcy-Forchheimer squeezed flow of Casson fluid over horizontal channel, Scientific Reports, **13**, 2666 (2023).

[20] Harshavardhan, A., Matt, S.B., Khan, M.I., Prakash, K.K., Alnuwaiser, M.A., Betageri, V.S. and Sidlinganahalli, M. Synthesis of Tin oxide nanoparticles using Nelumbo nucifera leaves extract for electrochemical sensing of dopamine, International Journal of Modern Physics B, (2022). https://doi.org/10.1142/S0217979223501084.

[21] Sivakumar, N., Tarakaramu, N., Satya Narayan, P.V. and Bhagya Lakshmi K. and Aruna Kumari, B. Three-dimensional magnetohydrodynamic Casson fluid flow over a linearly stretching surface: A numerical analysis, AIP Conference Proceeding, **2516**, 170022 (2022).

[22] Sivakumar, N. and Rushi Kumar, B. Comparative study of chemically reacting Blasius and Sakiadis unsteady MHD radiated flow with variable conductivity, J. Phys.: Conf. Ser. **1000**,012149 (2018).

[23] Harish Babu, D., Tarakaramu, N., Satya Narayana, P.V. and Sarojamma, G. and Makinde, O.D. MHD Flow and Heat Transfer of a Jeffrey Fluid over a Porous Stretching/Shrinking Sheet with a Convective Boundary Condition, International Journal of Heat and Technology, **39**, 885-894 (2021).

[24] Khashi'ie, N.S., Arifin, N.M. and Pop, I. Magnetohydrodynamics (MHD) boundary layer flow of hybrid nanofluid over a moving plate with joule heating, Alexndria Engineering Journal, **61**,1938-1945 (2022).

[25] Bourcy, S., Velizhanina, Y., Pavlenko, Y. and Knaepen, B. Optimal perturbations and transition in the magnetohydrodynamic boundary layer under the influence of a spanwise magnetic field, Physics of Fluids, **34**, 054115 (2022).

[26] Murad, M.A.S. and Hamasalh, F.K. Computational Technique for the Modelling on MHD Boundary Layer Flow Unsteady Stretching Sheet by B-Spline Function, 2022 International Conference on Computer Science and Software Engineering (CSASE), 236-240 (2022). Doi: 10.1109/CSASE51777.2022.9759738.

[27] Nasir, S., Berrouk, A.S., Aamir, A. and Gul, T. Significance of Chemical Reactions and Entropy on Darcy-Forchheimer Flow of H_2O and $C_2H_6O_2$ Convening Magnetized Nanoparticles, International Journal of Thermofluids, **17**, 100265 (2023).

[28] Jaafar, A., Waini, I., Jamaludin, A., Nazar, R. and Pop, I. MHD flow and heat transfer of a hybrid nanofluid past a nonlinear surface stretching/shrinking with effects of thermal radiation and suction, Chinese Journal of Physics, **79**,13-27 (2022).

[29] Gul, T., Usmam, M., Khan, I., Nasir, S., Saeed, A., Khan, A. and Ishaq, M. Magneto hydrodynamic and dissipated nanofluid flow over an unsteady turning disk, Advances in Mechanical Engineering, (2021). https://doi.org/10.1177/16878140211034392.

[30] Ahmad, F., Gul, T., Khan, I., Saeed, A., Mohamed Selim, M., Kumam, P. and Ali, I. MHD thin film flow of the Oldroyd-B fluid together with bioconvection and activation energy, Case Studies in Thermal Engineering, **27**, 101218 (2021).

[31] Bhagya Lakshmi, K., Sugunamma, V., Tarakaramu, N., Sivakumar, N. and Sivajothi, R. Cross-dispersion effect on magnetohydrodynamic dissipative Casson fluid flow via curved sheet, Heat Transfer, **51**,(2022).

[32] Satya Narayana, P.V., Tarakaramu, N., Sarojamma, G. and Animasaun, I.L. Numerical simulation of nonlinear thermal radiation on the 3D flow of a couple stress Casson nanofluid due to a stretching sheet, J. Thermal Sci. Eng. Appl. **13**,021028(2021).

[33] Sandhya, G., Malleswari, K., Sarojamma, G., Sreelakshmi, K. and Satya Narayana, P.V. Unsteady Casson nanofluid thin film flow over a stretching sheet with viscous dissipation and chemical reaction, Eur. Phys. J. Spec. Top. **230**, 1381-1390 (2021).

[34] Priam, S.S. and Nasrin, R. Numerical appraisal of time-dependent peristaltic duct flow using Casson fluid, International Journal of Mechanical Science, **233**, 107676 (2022).

[35] Shoaib, M., Kausar, M., Soopy Nisar, K., Zahoor Raja, M.A. and Morsy, A. Impact of thermal energy on MHD Casson fluid through a Forchhemier porous medium with inclined non-linear surface: A soft computing approach, Alexandria Engineering, **61**, 13311-12228 (2022).

[36] Riaz Khan, M., Johani, A.S.A., Elsiddieg, A. M. A., Saeed, T. and Mousa, A.A. A. The computational study of heat transfer and friction drag in an unsteady MHD radiated Casson fluid flow across a stretching/shrinking surface, International Communications in Heat and Mass Transfer, **130**, 105832 (2022).

[37] Gireesha, B.J., Shankaralingappa, B.M., Prasannakumar, B.C. and Nagaraja, B. MHD flow and melting heat transfer of dusty Casson fluid over a stretching sheet with Cattaneo-Christov heat flux model, International Journal of Ambient Energy, **43** (2022).

[38] Khan, U., Oudina, F.M., Zaib, A., Ishak, A., Baker, S.A., Sherif, E.S.M. and Baleanu, D. An exact solution of a Casson fluid flow induce by dust particle with hybrid nanofluid over a stretching sheet subject to Lorentz force, Waves in Random and Complex Media, (2022). https://doi.org/ 10.1080/17455030.2022.2102689.

[39] Shah, I.A., Bilal, S., Noeiaghdam, S., Gamiz, U.F. and Shahzad, H. Thermosolutal natural convection energy transfer in magnetically influence Casson fluid flow in hexagonal enclosure with fillets, Results in Engineering, **15**, 100584 (2022).

[40] Alzahrani, A.K., Abbas, Z. and Zaka Ullah, M. Chemically reactive two-phase flow of viscous-Casson fluids in a rotating channel, Alexandria Engineering Journal, **62**, 403-413 (2023).

[41] Raghunath, K. and Obulesu, M. Unsteady MHD oscillatory Casson fluid flow past an inclined vertical porous plate in the presence of chemical reaction with heat absorption and Soret effects, Heat Transfer, **51**, (2022).

[42] Bilal, M., Saeed, A., Gul, T., Kumam, W., Mukhtar, S. and Kumam, P. Parametric simulation of micropolar fluid with thermal radiation across a porous stretching surface; Comparative numerical analysis of Maxwell's time-dependent thermo-diffusive flow through a stretching cylinder, Scientific Reports, **12** (2022) 2542.

[43] Algehyne, E.A., Alhusayni, Y.Y., Tassaddiq, A., Saeed, A. and Bilal, M. The study of nanofluid flow with motile microorganism and thermal slip condition across a vertical permeable surface, Waves in Random and Complex Media, (2022). https://doi.org/10.1080/17455030.2022.2071501.

[44] Sandhya, G., Sarojamma, G., Satya Narayana, P.V. and Venkateswarlu, V. Buouyancy forces and activation energy on the MHD radiative flow over an exponentially stretching sheet with second-order slip, Heat transfer, **50**,(2021).

[45] Malleswari, K., Sarojamma, G., Sreelakshmi, K., Vijayalakshmi, R., Satya Narayana, P.V. and K. Vajravelu, Coupled effect of multi slips and activation energy in a micropolar nano liquid on a convectively heated elongated surface, Heat Transfer, **50**, (2021).

[46] Atwell, T.L., Townsend, P.A. and Grayson, M.N. Machine learning activation energies of chemical reactions, WIREs Comp. Mol. Sci. **12**, e1593 (2021).

[47] Azam, M., Xu, T., Nayak, M.K., Khan, W.A. and Khan, M. Gyrotatic microorganisms and viscous dissipation features on radiative Casson nanoliquid over a moving cylinder with activation energy, Waves in Random and Complex Media, (2022). https://doi.org/10.1080/17455030.2022.2112632.

[48] Tayyab, M., Siddique, I., Jarad, F., Ashraf, M.K. and Ali, B. Numerical solution of 3D rotating nanofluid flow subject to Darcy-Forchheimer law, bio-convection and activation energy, South African Journal of Chemical Engineering, **40**, 48-56 (2022).

[49] Sohail, M., Nazir, U., El-Zahar, E.R., Alrabaiah, H., Kumam, P., Mousa, A.A.A., Sitthithakerngkiet, K. and Choonkil, A. A study of triple-mass diffusion species and energy transfer in Carreau-Yasuda material influenced by activation energy and heat source, Sci. Rep. **12**, 10219 (2022).

[50] Ramesh, G.K., Madhukesh, J.K., Prasanna kumara, B.C. and Roopa, G.S. Significance of aluminium alloys particle flow through a parallel plate with activation energy and chemical reaction, J. Therm. Anal. Calorim. **147** (2022) 6971-6981.

[51] Zeeshan, A., Mehmood, O.U., Mabood, F. and Alzahrani, F. Numerical analysis of hydromagnetic transport of Casson nanofluid over permeable linearly stretched cylinder with Arrhenius activation energy, International Communications in Heat and Mass Transfer, **130**, 105736 (2022).
[52] Abbasi, A., Khan, S.U., Al-Khaled, K., Ijaz Khan, M., Farooq, W., Galal, A.M., Javid, K. and Malik, M. Thermal prospective of Casson nano-materials in radiative binary reactive flow near oblique stagnation point flow with activation energy applications, Chemical Physics Letters, **786**, 139172 (2022).
[53] Murshid, N., Mulki, H., Abu-Samha, M., Owhaib, W., Raju, S.S.K., Raju, C.S.K., Jayachandra Babu, M., Homod, R.Z. and Al-Kouz, W. Entropy Generation and Statistical Analysis of MHD Hybrid Nanofluid Unsteady Squeezing Flow between Two Parallel Rotating Plates with Activation Energy, Nanomaterials, **12**, 2381 (2022).
[54] Li, Y.X., Alqsair, U.F., Ramesh Khan, S.U. and Imran Khan, M. Nonlinear Heat Source/Sink and Activation Energy Assessment in Double Diffusion Flow of Micropolar (Non-Newtonian) Nanofluid with Convective Conditions, Arab. J. Sci. Eng. **47**, 859-866 (2022).
[55] Dhlamini, M., Mondal, H., Sibanda, P. and Motsa, S. Activation energy and entropy generation in viscous nanofluid with higher order chemically reacting species, International Journal of Ambient Energy, **43**, (2022).
[56] Samuel, D.J., Adegbie, K.S. and Omowaye, A.J. Significance of non-uniform heat generation and convective boundary conditions in heat and mass transfer flow of Jeffrey fluid in the presence of Arrhenius activation energy and binary reaction, Eur. Phys. J. Spec. Top. **232**, 877-891, (2023).
[57] Bilal, M., Alduais, F.S., Alrabaiah, H. and Saeed, A. Numerical evaluation of Darcy Forchhemier hybrid nanofluid flow under the consequences of activation energy and second-order chemical reaction over a slender stretching sheet, Waves in Random and Complex media, (2022). https://doi.org/10.1080/17455030.2022.2111477.
[58] Algehyne, E.A., Saeed, A., Arif, M., Bilal, M., Kumam, P. and Galal, A.M. Gyrotactic microorganism hybrid nanofluid over a Riga plate subject to activation energy and heat source: numerical approach, Scientific Reports, **13,** 13675(2023).
[59] Thammanna, G.T., Ganesh Kumar, K., Gireesha, B.J., Ramesh, G.K. and Prasannakumara, B.C. Three dimensional MHD flow of couple stress Casson fluid past an unsteady stretching surface with chemical reaction, Results Physics, **7**, 4101-4110 (2017).
[60] Wang, C.Y. The three-dimensional flow due to a stretching sheet, Phys. Fluids, **27** 1915-1917 (1984)
[61] Hayat, T., Shehzad, S.A. and Alsaedi, A. Three-dimensional stretched flow of Jeffrey fluid with variable thermal conductivity and thermal radiation, Appl. Math. Mech. Engl. Ed., **34**, 823-832 (2013).
[62] Ibrahim, F.N. and Terbeche, M. Solutions of the laminar boundary layer equations for a conducting power law non-Newtonian fluid in a transverse magnetic field, J. Phys. D Appl. Phys., **27**(4), 740-747 (1994).
[63] Dimian, M.F. Effect of the magnetic field on forced convection flow along a wedge with variable viscosity, Mech. Mech. Eng., **7**,107-120(2004).
[64] Sarah, I., Mondal, S. and Sibanda, P. Unsteady Casson nanofluid flow over a stretching sheet with thermal radiation, convective and slip boundary conditions, Alexandria Eng. J., **55**, 1025-1035 (2015).
[65] Nadeem, S., Haq, R.U., and Akbar, N.S. MHD three-dimensional boundary layer flow of Casson nanofluid past a linearly stretching sheet with convective boundary condition, IEEE Trans. Nanotech. **13**, 109-115 (2014).
[66] Gupta, S. Sharma, K. Numerical simulation for magnetohydrodynamic three-dimensional flow of Casson nanofluid with convective boundary conditions and thermal radiation, Eng. Comp. **34**, 2698-2722 (2017).
[67] Ahmad, K. and Nazar, R. Magnetohydrodynamic three-dimensional flow and heat transfer over a stretching surface in a viscoelastic fluid is discussed, J. Sci. Technol.**3**, (2011).

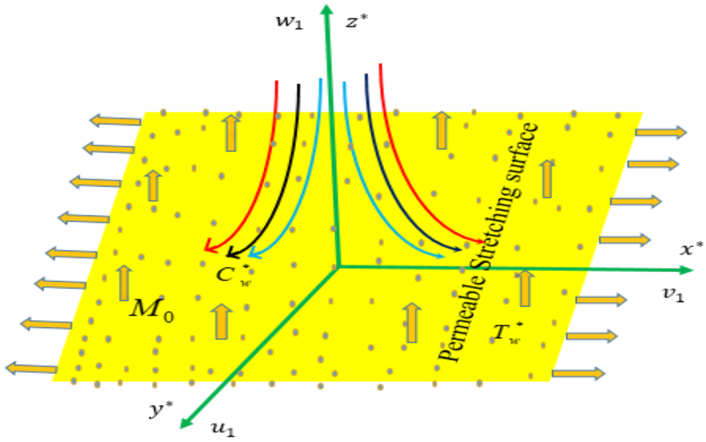

Fig. 1 Physical Model of the Problem / Graphical Abstract

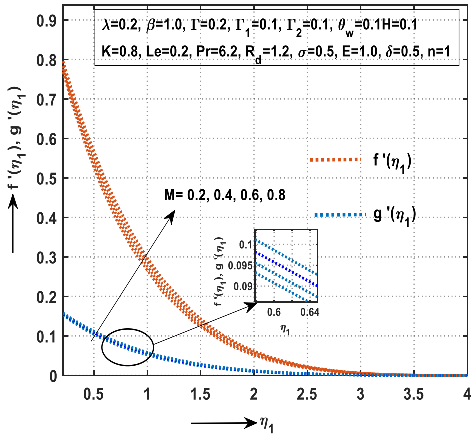

Fig.2 The variation of M on $f'(\eta_1)$ and $g'(\eta_1)$

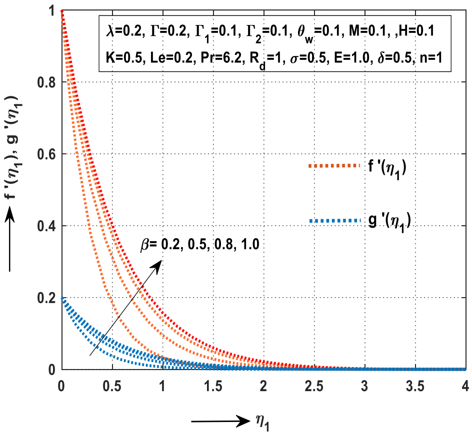

Fig. 3 The variation of β on $f'(\eta_1)$ and $g'(\eta_1)$

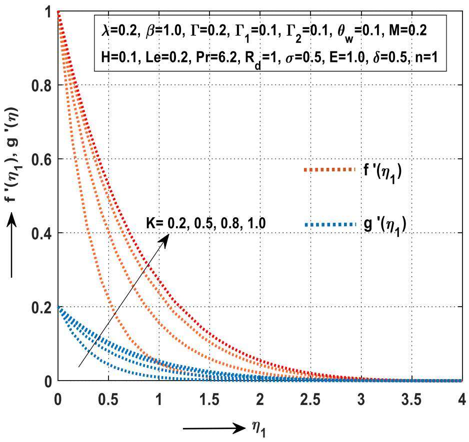

Fig. 4 The variations of K on $f'(\eta_1)$ and $g'(\eta_1)$

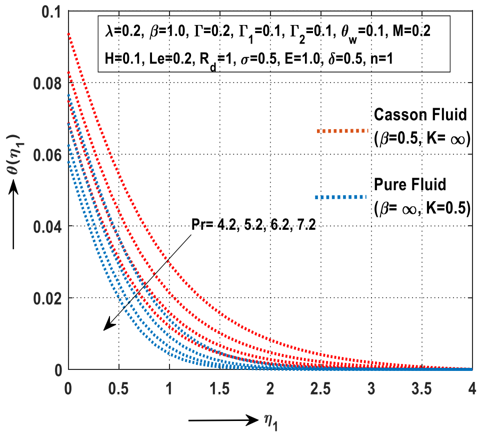

Fig. 5 The variations of $\Pr$ on $\theta(\eta_1)$

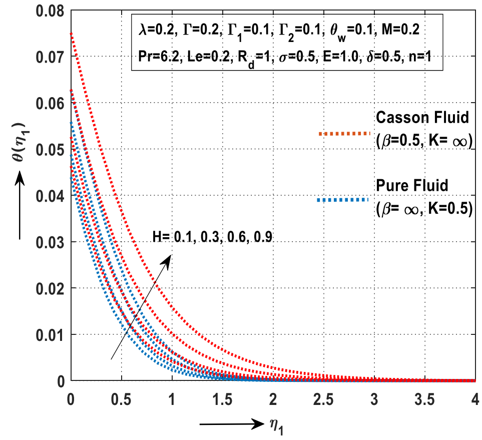

Fig. 6 The variations of H on $\theta(\eta_1)$

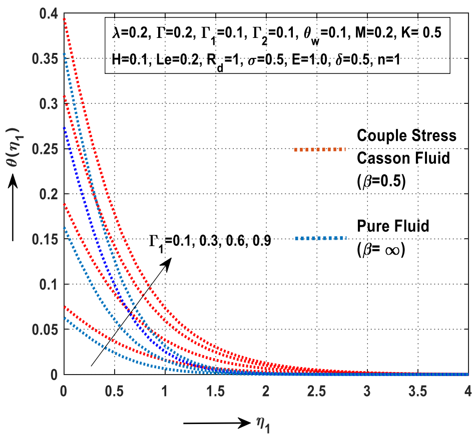

Fig 7 The variations of Γ_1 on $\theta(\eta_1)$

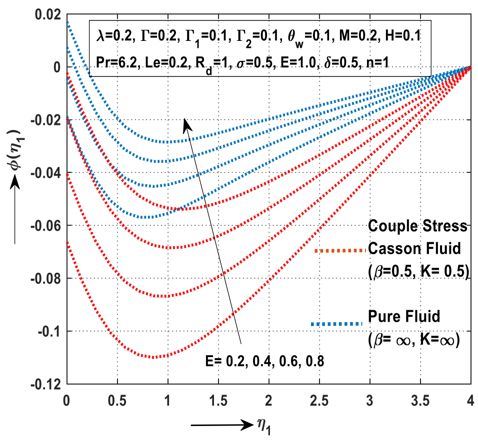

Fig 8 The variations of E on $\phi(\eta_1)$

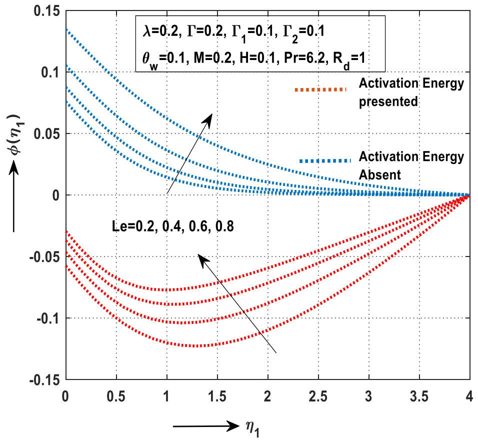

Fig 9 The variations of Le on $\phi(\eta_1)$

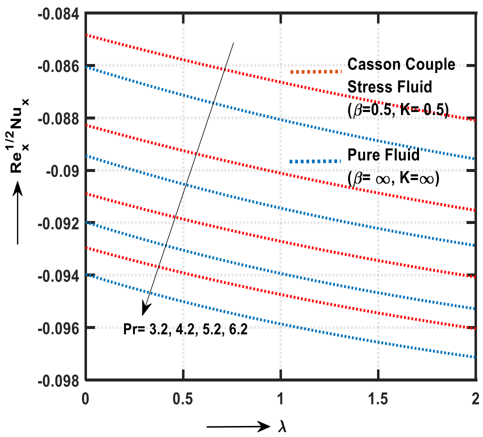

Fig 10 The variations of Pr on $\mathrm{Re}_x^{-1/2} Nu_x$

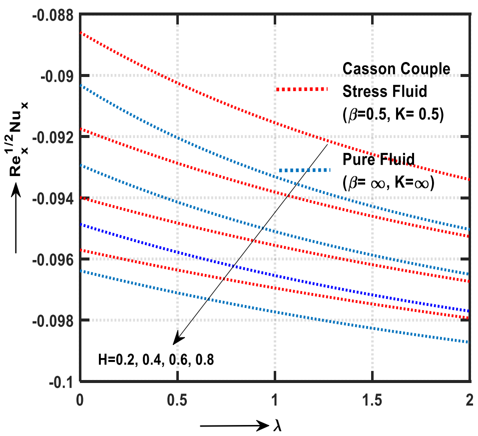

Fig 11 The variations of H on $\mathrm{Re}_x^{-1/2} Nu_x$

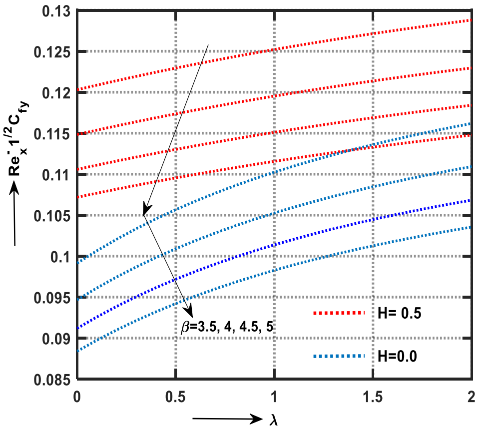

Fig 12 The variation of β on $\mathrm{Re}_x^{1/2} C_{fx}$

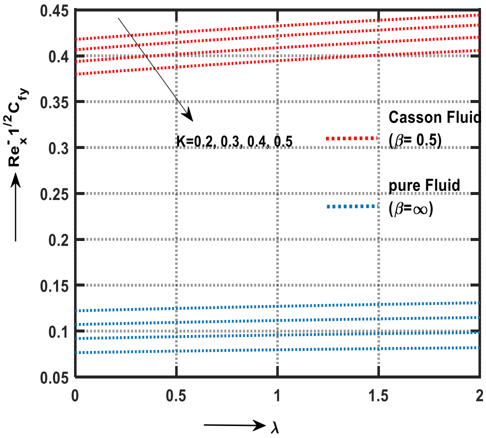

Fig 13 The variations of K on $\mathrm{Re}_x^{1/2} C_{fy}$

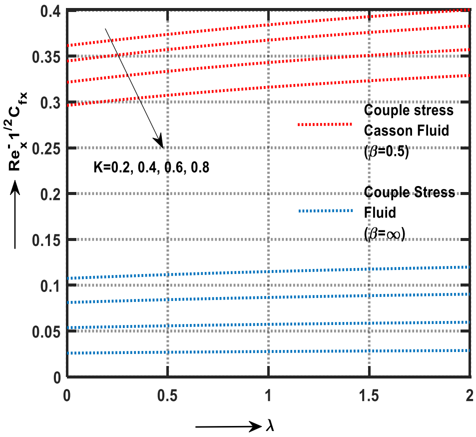

Fig. 14 The variations of K on $\mathrm{Re}_x^{1/2} C_{fx}$

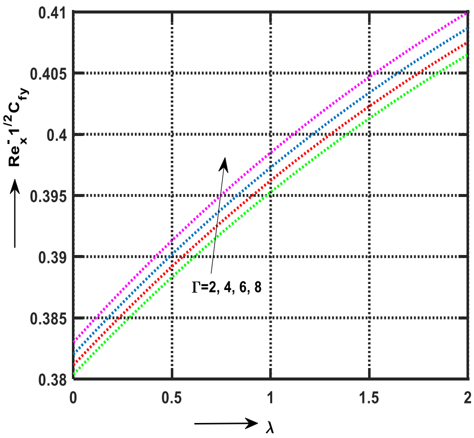

Fig. 15 The variations of Γ on $\mathrm{Re}_x^{1/2} C_{fy}$

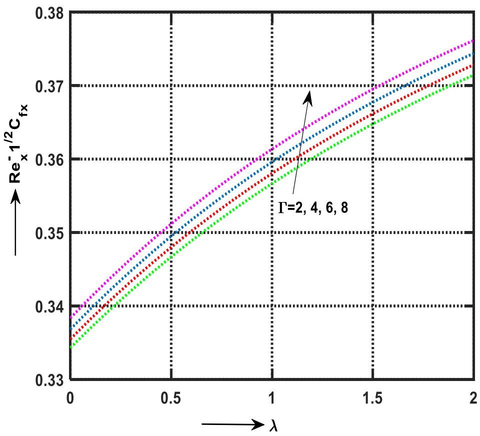

Fig. 16 The variations of Γ on $\mathrm{Re}_x^{1/2} C_{fx}$

Table. 1 Evaluation of Skin friction coefficient $\left(1+\frac{1}{\beta}\right) f''(0)$ for $K=0$.

M	β	Present study	Sarah et	Nadeem et	Gupta et al.	Ahmad et al.

			al. [64]	al. [65]	[66]	[67]
0.0	∞	1.000000000	1.00000	1.0004	1.0003181	1.0042
	1.0	1.414214608	1.41421	1.4142	1.4142136	-
	2.5	1.183215995	-	-	-	-
	3.5	1.133893450	-	-	-	-
	5.0	1.095445140	1.09544	1.0954	1.0954675	-
10	∞	3.316624790	3.31662	3.3165	3.3165824	3.3165
	1.0	4.690415759	4.69042	4.6904	4.6904349	-
	2.5	3.924283374	-	-	-	-
	3.5	3.760699028	-	-	-	-
	5.0	3.633180449	3.63318	3.6331	3.6331824	-
100	∞	10.04987561	10.04987	10.049	10.049864	10.049
	1.0	14.21670403	14.21267	14.2127	14.212668	-
	2.5	11.89117045	-	-	-	-
	3.5	11.39548790	-	-	-	-
	5.0	11.00908715	11.00909	11.0091	11.009112	-

[68]

Table. 2 Comparison of Skin friction coefficient for $K = 0$ and $\lambda = 1.0$

M	β	**Present study**	**Nadeem et al. [65]**
0.0	∞	1.173719025	--
	1.0	1.659891956	1.6599
	2.5	1.388765332	--
	3.5	1.330874747	--
	5.0	1.285747074	1.2857
10	∞	3.367222224	3.3667
	1.0	4.761964421	4.7620
	2.5	3.984161191	--
	3.5	3.818079080	--
	5.0	3.688613149	3.6886
100	∞	10.06646642	10.066
	1.0	14.23613181	14.2361
	2.5	11.91079007	---
	3.5	11.41428580	---
	5.0	11.55856650	11.0272

Nomenclature	
a_1 Channel length	τ_w wall shear stress
b_1 Thermal slip parameter	(u_1, v_1) Velocity components along x and y-axes
u_1, v_1, w_1 velocity components along x^*, y^*, z^*	(x^*, y^*) Cartesian coordinate's
C^* Nanoparticle volume fraction	U_w^* Stretching velocity
C_∞^* Uniform ambient concentration	U_∞^* Free stream velocity

C_f^* Skin friction coefficient	***Greek symbols***
C_p^* Specific heat constant	α_m^* Base fluid thermal diffusivity $= k/(\rho C)_f$
C_w^* Variable concentration	η_1 Similarity variable
c_p Specific heat at constant pressure	μ Dynamic viscosity
D_n Variable microorganism diffusion coefficient	ϕ Dimensionless concentration
D_T Thermophoresis diffusion	λ Ratio parameter $= b_1 / a_1$
D_B Brownian diffusion	υ^* Kinematic viscosity $= \mu / \rho_f$
E Activation Energy $= \frac{Ea}{KT}$	δ Temperature Difference Parameter
f Dimensionless stream function	σ Reaction Rate $= \frac{K_r^2}{B}$
f' Dimensionless velocity	θ Dimensionless temperature
H Heat source parameter $\frac{Q_0\left(T^* - T_\infty^*\right)}{(\rho C)_f}$	ρ_s density of the solid
K Couple Stress Parameter $= \frac{a_1\left(\upsilon^*\right)'}{\left(\upsilon^*\right)^2}$	Γ_1, Γ_2 Temperature and concentration Biot Numbers respectively $\Gamma_1 = \frac{h_1}{k}\sqrt{\upsilon^* / a_1}$, $\Gamma_2 = \frac{h_2}{k}\sqrt{\upsilon^* / a_1}$
Le Lewis number $= \frac{\alpha_m^*}{D_B}$	Γ Porous parameter $= \frac{\upsilon^*}{a_1 k_p}$
M magnetic field parameter $= \frac{\sigma^* M_0^2}{a_1 \rho_f}$	$\left(\upsilon^*\right)'$ Couple stress parameter $= \eta_1 / \rho_f$
$\Pr$ Prandtl number $= \left(\frac{\upsilon^*}{\alpha_m^*}\right)$	υ^* Kinematic viscosity
Re_x Reynolds number	σ^* Boltzmann constant
T^* Fluid temperature	γ Chemical reaction parameter $= K_1 / a_1$
T_0^* constant Temperature at zero	ρ Fluid density
T_1^* Temperature on lower wall	ρ_f Fluid density
T_2^* Temperature on upper wall	***Subscripts***
T_∞^* fluid temperature far away from the surface	∞ condition at free stream
T_w^* Constant fluid Temperature of the wall	w wall mass transfer velocity
Abbreviations	

HMTR Heat and Mass Transfer Rate	CSC Couple Stress Casson
NFs Nanofluids	SS Stretching Sheet
PDE Partial Differential Equations	ODE Ordinary Differential Equations
AE Activation Energy	TR Thermal Radiation
CR Chemical Reaction	PSS Porous Stretching Sheet
HNFs Hybrid Nanofluids	BL Boundary Layer
SR Shear Rate	NPs Nanoparticles
HT Heat Transfer	TC Thermal Conductivity
NN Nonnewtonian	NLTR Nonlinear Thermal Radiation
CFM Casson Fluid Motion	TE Thermal Energy
HNFs Hybrid Nanofluids	AAE Arrehenius Activation Energy
HG Heat generation	MF Magnetic Field
PM Porous Medium	NUHG Nonuniform Heat Generation
DF Darcy-Forchheimer	PS Porous Space
OH Ohmic heating	KV Kinematic Viscosity
TD Thermal Diffusivity	EPG Electrical Power Generation
ML Micropolar Liquid	PG Power Generation
NPP Nuclear Power Plants	WBNFs Water Based nonfluids